Published in final edited form as:
J Mol Biol. 2007 November 9; 373(5): 1334–1347.

A Fluid Salt-Bridging Cluster and the Stabilization of p53 ⋆

ThuZar Lwin[a,1], **Jason J. Durant**[b,a,1,3], and **Donald Bashford**[a,1,2,*]

a*Saint Jude Children's Research Hospital, Hartwell Center for Bioinformatics and Biotechnology, 322 N. Lauderdale St., Mail stop 312, Memphis, TN 38105*

b*Department of Physics, University of Memphis, Memphis, TN*

Abstract

p53 is a homotetrameric tumor suppressor protein that is found to be mutated in most human cancers. Some of these mutations, particularly mutations to R337 fall in the tetramerization domain and cause defects in tetramer formation leading to loss of function. Mutation to His at this site has been found to destabilize the tetramer in a pH-dependent fashion. In structures of the tet domain determined by crystallography, R337 from one monomer makes a salt bridge with D352 from another monomer, apparently helping to stabilize the tetramer. Here we present molecular dynamics simulations of wild-type p53 and the R337His mutant at several different pH and salt conditions. We find that the 337–352 salt bridge is joined by two other charged sidechains, R333 and E349. These four residues do not settle into a fixed pattern of salt-bridging, but continue to exchange salt-bridging partners on the nanosecond timescale throughout the simulation. This unusual system of fluid salt-bridging may explain the previous finding from alanine scanning experiments that R333 contributes significantly to protein stability even though, in the crystal structure it is extended outward into solvent. This extended conformation of R333 appears to be the result of a specific crystal contact and, this contact being absent in the simulation, R333 turns inward to join its interaction partners. When R337 is mutated to His but remains positively charged, it maintains the original interaction with D352, but the newly observed interaction with E349 is weakened, accounting for the reduced stability of R337H even under mildly acidic conditions. When this His is deprotonated, the interaction with D352 is also lost, accounting for the further destabilization observed under mildly alkaline conditions.

Simulations were carried out using both explicit and implicit solvent models, and both displayed similar behavior of the fluid salt-bridging cluster, suggesting that implicit solvent models can capture at least the qualitative features of this phenomenon as well as explicit solvent. Simulations under strongly acidic conditions in implicit solvent displayed the beginnings of the unfolding process, a destabilization of the hydrophobic dimer–dimer interface. Computational alanine scanning using the MM/PBSA method showed significant correlation to experimental unfolding data for charged and polar residues, but much weaker correlation for hydrophobic residues.

⋆We thank Richard Kriwacki and Charles Galea for helpful discussions and advance access to NH-exchange data. Computing resources were provided by the Hartwell Center for Bioinformatics and Biotechnology.

*Corresponding author *Email addresses:* thuzar.lwin@stjude.org (ThuZar Lwin), jason.j.durant@vanderbilt.edu (Jason J. Durant), don.bashford@stjude.org (Donald Bashford).

[1]Supported by the American Lebanese Syrian Associated Charities, Inc. (ALSAC)
[2]Supported by the National Institutes of Health (GM57513).
[3]Present address: Vanderbilt University, College of Medicine

Keywords

p53; MM/PBSA; Generalized Born; salt bridge; salt bridge exchange; molecular dynamics; protein flexibility; tetramerization domain; acid unfolding; destabilization; computational alanine scanning

1 Introduction

The human tumor suppressor p53, known as the "guardian of genome," is a transcription factor involved in a number of cellular functions such as DNA repair, apoptosis, cell-cycle arrest and transcription of its regulator, MDM2,[1,2]. Activation of p53 can be triggered by a number of events such as DNA damage[3,4], hypoxia, hyperthermia and suboptimal cellular growth conditions[2,5]. The p53 monomer consists of five structural and functional domains: the N-terminal trans-activation domain, a proline rich regulatory domain, the DNA-binding domain, the tetramerization domain and the C-terminal regulatory domain. The active form of p53 is a homotetramer and the tetramerization (tet) domain is responsible for this oligomerization.

The structure of the tet domain has been solved by both NMR[6-8] and X-ray crystallography[9-11]. The tetramer is a dimer of dimers in which the 32 residues of the monomer (325 to 356) form a V-shaped structure with one arm in a beta-strand conformation and the other in an alpha-helical conformation. The dimers are formed from two monomers related by a two-fold rotational axis forming a two-stranded, anti-parallel beta sheet packed against one side of a pair of anti-parallel alpha helices. Another two-fold axis relates the two dimers of the tetramer so as to pack the other sides of their helix pairs at an angle of 81°, thus forming a sandwich of four alpha helices between two double-stranded beta sheets as shown in Figure 1A. Of particular interest here are four identical ionic interaction sites in which R337 and D352 form a salt bridge in the crystal structure, as shown in Figure 1B. These are thought to be important in stabilizing the complex[9].

The tetrameric complex plays important functional roles in many cellular transformations[12]. Although binding to DNA occurs through the DNA-binding domain, defects in the tet domain can also have deleterious effects. It has been reported that p53 monomers without the tet domain bind to DNA with a 10 to 100-fold reduced binding affinity relative to the full length p53, and that there are significant differences in the bending and twisting of DNA upon binding[13,14]. p53's activity as a transcription factor relies on certain residues in the tet domain for its sequence-specific trans-activating function[15]. One example is the human homologue of checkpoint kinase which prefers tetrameric over monomeric p53 to phosphorylate Ser20 after DNA damage, and deletion of the tet domain completely eliminates its phosphorylation activity[16]. Proper tetramerization is also critical for the ubiquitination by MDM2 in regulating cellular level of p53. The tet domain-defective mutant monomers show drastic reduction in sensitivity to MDM2-mediated degradation compared to the wild type tetramers[17,18].

The tet domain can also interact directly with other proteins. It interacts with Ca^{2+}-dependent protein-kinase-C and promotes sequence-specific binding of the DNA core domain[19]. On the other hand, the adenovirus E4orf6 can bind to the tet domain of p53 and inhibit p53-mediated transcriptional activity[20]. The tetrameric complex of p53 also influences its subcellular localization. Part of the tet domain, residues 340 to 352, is in fact the nuclear export signal, but is buried within the hydrophobic core of the tetramer. This nuclear export signal becomes exposed when p53 is in either monomeric or dimeric form, making it easily accessible by nuclear exportin 1, leading to export from the nucleus and degradation[21].

Mutations in the tet domain can cause tetramer instability[22-24] or the complete loss of tetramer formation[25]. Tumors associated with germline mutation in tet domain are shown in figure 2A,

along with the frequency of mutation (both germline and somatic) in each residue in figure 2B. In particular, R337H has been linked to pediatric adrenocortical carcinoma (ACC) in a population of children in southern Brazil[26]. Biological and biophysical assays show that R337H has a DNA binding affinity and structure similar to wild type, although the tetrameric complex is somewhat less stable[22,26]. However, while the wild type's stability is pH insensitive over the range 5–9, the mutant becomes destabilized as the pH is raised from 7 to 8. This pH dependence is found to correlate with the titration of the histidine residue, leading to the proposal that disruption of a salt bridge between R/H337 and D352 is responsible for the destabilization[22]. In addition the R337H mutant can form amyloid fibrils *in vitro*[23,24], with the G334V mutant being the only other tet-domain mutant known to form fibrils[27]. This direct clinical relevance has led us to further investigate R337H, as well as the wild type, by molecular dynamics simulation.

Formation of the native p53 tetramer has been studied at different levels. At the cellular level, a biogenesis study on the full length peptide reported that p53 dimers are formed co-translationally while tetramers are formed post-translationally[28]. It is reasoned that the spatial closeness leads to dimers, as nascent p53 chains interact with each other before being released from the polysomes. In *in vitro* kinetic studies, the folding mechanism has been determined to consist of two steps. First the unstructured monomers form a transient dimeric state, which then undergoes molecular reorganization to form a second transient dimeric intermediate (STDI). Finally, two STDIs associate to form a native tetramer[29].

The folding of the tet domain has been studied computationally by two groups[30,31], each focusing on a different step of folding. Chong and coworkers[30] focused on the process of dimerization using large numbers of partial unfolding simulations in explicit water at 470K, followed by refolding simulations at normal temperature. Analysis of these trajectories was used to characterize the transition-state ensemble of the dimer-forming process. The same group used similar techniques to do a novel type of computational alanine scanning[32]. On the other hand, Duan and Nilsson[31] studied the unfolding mechanism of the full tetramer, including the tetramer-to-dimer transition, using implicit solvation and repeated simulation at elevated temperatures. The ϕ values calculated from statistical analysis of these simulations were reported to be in fair agreement with those of an experimental refolding study[29]. It was suggested that the way the tetramer complex forms closely resembles the folding of intrinsically unstructured proteins, which become folded only upon association with other proteins[33,34].

Here, we present simulations and analysis of the tetramer at 300 K for both the wild type and the R337H mutant, including simulations of several different pH and salt conditions. The focus of these studies is to identify factors contributing to the stability of the tetramer, with particular focus on the role of R337 and other salt-bridge forming residues. We found that at each of the four monomer–monomer interacting sites, R337 and D352, which are seen in a salt bridge in the crystal structure[9], are joined by R333 and E349 forming an ionic network among R333, R337, E349 and D352. A detailed analysis of the interchanges among salt-bridging partners gives a more complex and fluid view of their role than analysis of only the crystal structure. Simulations using both the conventional explicit-water representation of solvation and the generalized-Born (GB) method, an implicit-solvent method in which explicit water is replaced by a continuum[35], are performed and compared, giving a test of the GB method in a system with complex and dynamic salt-bridges. A computational alanine scanning method based on MM/PBSA techniques[36] is used to estimate the result of all possible sidechain truncations to alanine and compared with experimental alanine scanning data[25].

Results and Discussion

Molecular dynamics simulations of the wild-type and mutant *tet* domain were performed using both explicit solvent and the GB implicit solvation model to study the effects of both the simulation methods and solution conditions. For the R337H mutant, neutral to mildly acidic conditions were simulated by protonating H337, while mildly alkaline conditions were simulated by deprotonating this residue. There are no other His residues in the protein, nor are there Cys or other residues likely to titrate in the neutral range. In simulations for mild pH conditions all Glu, Asp, Lys and Arg are put in their charged states in all simulations. In simulations for strongly acidic conditions, Asp and Glu residues are neutralized. In the implicit-solvent simulations, varying salt concentration was simulated via the extended GB model of Srinivasan et al.[37] The temperature in all simulations is 300K. The various combinations of simulation methods and conditions, together with the abbreviations used to denote the different runs are given in Table 1.

Structural Equilibration and Stability

General—GB simulations were continued for 15 ns of production simulation after the 1 ns of equilibration described in Methods, while the explicit water simulations, which sample conformational space more slowly, were continued past the preliminary equilibration described in Methods for 20 ns, and the designation of further equilibration versus production phases was made by inspection of the stability of the simulation. Figure 3 shows the backbone RMSDs of the simulated trajectories with respect to the X-ray structure. The preceding 1.0 ns equilibration phase was sufficient for the GB simulations, as demonstrated by the RMSDs fluctuating about 2.5 Å throughout the production run. In the case of the explicit water simulations, wherein the preliminary equilibration steps totaled only 160 ps (see Methods), another 7.0 ns were required to reach to equilibrium RMSD (Figure 3). Therefore only the last 13.0 ns of the 20 ns plotted in Figure 3 was considered as the production run. The fact that both explicit and implicit solvent simulations equilibrate to very similar RMSD values, as well as visual inspection and quantitative analysis of the trajectories, show that, with two exceptions, the GB runs were in good agreement with the explicit solvent. The two exceptions were the GB runs corresponding to acid unfolding conditions.

Acid destabilization—As seen in figure 3, RMSDs of the GB acidic simulation went as high as 9.0 Å for the wild-type and 7.0 Å for the mutant. More detailed inspection of these trajectories (see supplemental figures) showed that contributing factors to the high RMSD included change in angle between dimers, partial helix unwinding and loosening of the hydrophobic core. Thus the high RMSD value does not necessarily correlate to peptide unfolding as might be the case for single peptides. In particular the high RMSD value of the tetramer in the wild-type acidic simulation is largely attributable to dimer rotation. Following the procedure of Duan and Nilsson[31], the hydrogen bond from the backbone CO group of E339 to the backbone NH group of E343 is considered as the vector to measure the angle between dimers. In the crystal structure, helix A in dimer AB makes an 84° angle (∠HA:HD) with helix D in dimer CD, and the same holds true for helices B and C (∠HB:HC). However ∠HA:HD and ∠HB:HC fluctuations dramatically shifted from the vicinity of 80° to 140° near 7.5 ns in GB/0.1M/Wt+. In GB/0.1M/Mut+, the rotation is not as apparent as in the wild type, but appears to be moving back and forth between 60° and 120°.

In addition to the rotational deviations, a loosening of the hydrophobic core between the dimers was observed. As an indicator of translational motions between dimers, the distance between the C_α atoms of A347 of monomers A and D, and the analogous distance between monomers B and C, were chosen (see supplemtnal figures). This distance in crystal structure is 5.01 Å, and A347 has previously been identified experimentally as a residue involved in the

hydrophobic dimer–dimer interface and important for stability[25]. Much of the deviation from 5.01 Å is due to the dimer rotation discussed above. However significant deviations from the crystal-structure distance were also seen when the dimer angle, ∠HA:HD was near its crystal-structure value of 84°. In particular, the A347[A:D] distance reached up to 12.5 Å in GB/0.1M/Mut+ near 2.5 ns and remained at a large distance for another 1.5 ns. During this same time period, the dimer angle ∠HA:HD was near 84°. Therefore the large A347[A:D] value is interpreted as a helix lifting away from the tetramer core. Visual inspection confirmed this, and also led to the observation of large transient increases in the solvent exposure of M340, L344, A347 and L348. It was also observed that the dimer–dimer interaction, L350–L350, was absent about 50% of the time. While it seems unremarkable for M340 and L348 to be exposed to the solvent as they are only partially buried in the hydrophobic core even in the crystal structure, exposure of L344 and A347 to the solvent indicated a more marked loosening of hydrophobic core. The loosening observed here could not be captured by monitoring the radius of gyration of hydrophobic core residues, which is a more general but coarse-grained measure (data not shown). Rather, monitoring more specific structural details, such as those described above, was required.

As for the internal structure of the dimers, the monomer helices did not stay anti-parallel to each other all the time. This is monitored by the inter-helical distance from C_α of N345 on one helix to C_α of R337 on another helix within a dimer (see supplemental figures). Two such distances are measured within each dimer. If the helices within a dimer (dimer AB for example) are anti-parallel to each other, the N345 to R337 distance from helix A to B should be the same as that from helix B to A. In the crystal structure symmetry makes the helices perfectly anti-parallel and the distances are both 8.77 Å. N345 was chosen to avoid effects of the helical unwinding at E346 as described below. Both wild-type and mutant show fluctuations in helical distance within corresponding dimers. However, the fluctuation is more pronounced in GB/0.1M/Mut+ than in GB/0.1M/Wt+, suggesting that the shorter sidechain of H337 in mutant could be causing the large fluctuation. We believe this event is due to the pocket formation resulting from shorter sidechain of H337 followed by loss of the ionic network, which will be discussed later, exacerbating the dimer instability. The fluctuations in non-acidic simulations were much smaller.

As for the secondary structure stability of individual monomers, partial helical unwinding at the C-terminus was observed in both wild-type and mutant under acidic conditions upon visual inspection. The helical unwinding was followed by re-formation of helix either with a kink or with a reverse turn. For the mutant the kink occurred at E346, and for the wild-type at E349 with a reverse turn. This partial helix instability appears to be due to the loss of sidechain interactions between R342 and other negatively charged residues on the monomer helix. In non-acidic conditions, R342 stabilizes the helix by interacting with sides chains of E339, E343 and E346 within a monomer. However when the sidechains of these glutamate residues are protonated in acidic simulation, they are no longer available to interact with R342 causing the helix to become unstable. Such unwinding was not seen in the non-acidic simulations.

The above results are consistent with the experimental finding that the wild-type tetramer is quite stable at pH 7 (T_m = 84.5°C), but much less stable at pH 3 (T_m = 34.3°C)[38]. On the other hand, the mutation, R337H, which causes T_m to drop to 32°C at pH 9[22], simulated with H337 either protonated or not did not lead to gross deviations from the native fold. However, as discussed below, it did lead to changes in salt-bridging.

Duan and Nilsson[31] found that in unfolding simulations at high-temperature (500 K and 600 K), unfolding started with disruption of the dimer–dimer interface, and that disruption of this interface is accompanied by significant distortions of the dimer structures such that by the time this interface was broken, the free dimers had little resemblance to the dimers in the folded

tetramer. The transition-state ensemble was found to be near the folded state, but with substantial disruption of the hydrophobic core. In this context, our simulations under conditions of room temperature and acidic pH seem to be to coming near the unfolding transition state identified by these workers.

Salt-Bridging Network and Solvent Models

Fluid ionic cluster—The salt-bridge interaction of R337 with D352 has been observed in the X-ray structure[9], and its disruption is thought to be the mechanism whereby mutation of R337 destabilizes the tetramer. However, during the simulations we found in the region of this salt bridge, an ionic network involving all possible +/- pairings of R333, R337, D352 and E349. The participation of R333 is particularly striking since in the crystal structure, this residue is extended into solvent and far from the above residues (Figure 1B), while in alanine scanning experiments[25] it is found to contribute significantly to protein stability. Instead of remaining in this extended conformation, R333 rotated its C_γ-C_δ and C_δ-N_ε bonds to bend its guanidinium head inward, which was then inserted between sidechains of E349 and D352 of the monomer with which it forms a dimer (Figure 1C).

The re-orientation of R333 started early in the equilibration stage. Figure 4A shows the instantaneous distances at the AB interaction site observed in the trajectory GB/0.1M/Wt (see Figure 1 for the interaction-site nomenclature). The distance was calculated from either the guanidinyl carbon (C_ζ) of arginine or the center of mass of N_δ+N_ε of histidine to the carbonyl carbon of the acidic sidechain. By this metric a distance less than 5 Å is sufficient to form a salt bridge. Unless otherwise stated, this type of interaction distance will simply be referred to as the distance between two named residues. As shown in figure 4A, in the beginning R333 was approximately 8.0 Å from either E349 or D352. But after 50 ps of equilibration, the R333-E349 and R333-D352 interactions were formed and their distances were decreased to 4 or 5 Å. Notice at this site that the R337-D352 interaction was retained throughout the equilibration and almost no interaction exists for R337-E349. However a completely opposite situation, in which no R337-D352 but R337-E349 along with one or both of the other two interactions, could occur at sites BA, CD or DC. Overall this ionic interaction among the four residues is the typical behavior observed in all simulation conditions with varying frequency, except for the strong acid simulations in which Glu and Asp residues were protonated.

Figure 4B(i) shows the site-AB salt-bridging distances from the production phase that was continued from the equilibration phase of Figure 4A, while Figures 4B(ii-iv) show the corresponding differences from the other three symmetry-related interaction sites. Most of the time, three of the four possible oppositely-charged pairs have distances of 5.5 Å or less, while the fourth distance is 6.0 Å or more. For example, at approximately 3.0 ns into the production run, the R337-E349 interaction in the AB site (red trace in Figure 4B(i)) began to form and its interaction remained intact throughout the trajectory. At the same time however, the R333–E349 distance (green trace) increased from 4 Å and 8-10 Å while that of R333–D352 (blue trace) remained less than 5 Å throughout the simulation. Visualization of this event showed that a rotation of nearly 180° about the C_δ– N_ε bond of R333 swings the guanidinium group outward away from E349 while preserving an H-bonding interaction between the N_ε atom and a carboxylate oxygen atom of D352. Examination of other trajectory snapshots showed that pairs that were close by our chosen metric were often, but not always involved in conventional hydrogen-bonding. Other geometries were closer to π-stacking between the carboxylate and guanidinium functionalities. When R333 formed interactions either with E349 or D352, it did not necessarily disrupt the interaction of R337 with the same acidic residue. For example, in sites BA and CD, E349 interacted strongly with both arginine residues (green and red traces in figure 4B(ii and iii)), while in site DC, D352 interacted with both arginine residues (figure 4B(iv), blue and black traces).

While R333 was not observed to return to the extended, solvent-exposed conformation of the X-ray structure in the GB/0.1M/Wt simulation plotted in Figure 4, or in the GB/0.0M/Wt simulation, a short return of 10.0 to 40.0 ps was observed in the GB/0.1M/Mut- and GB/01.M/Mut simulations. In acidic GB and explicit water simulations, we observe a longer period of R333 returning to extend back into the solvent.

Comparison among solvent models—Figure 5 shows the distance distribution of interactions for all simulations performed. The general features of the wild-type simulation at neutral pH are similar across the three different solvent/electrolyte models, explicit/Wt, GB/0.0M/Wt and GB/0.1M/Wt. R337–E349 had the strongest salt-bridging peak in the wild-type simulations. R333–E349 was the second most populated, but the peak is slightly shifted to a shorter distance. The interaction seen in the X-ray structure, R337–D352, was relatively weak in all three of these simulations, showing a significant peak at a longer distance (6 to 7 Å). Some differences among the simulations are seen on closer analysis. The R337–D352 pair was rarely seen at short distance in the GB/0.0M/Wt and Explicit/Wt runs, while in GB/0.1M/Wt did it have a significant population of short-range interactions. The slow timescale of swapping events makes it difficult to assess the significance of these differences.

Mutation and pH dependence—Figure 5 also shows distance distributions from the simulations corresponding to the R337H mutant and to different pH conditions (Table 1). When R337 was mutated to histidine in GB simulations, the R333– E349 and R333–D352 interactions were not disrupted in the GB/0.1M/Mut- and GB/0.1M/Mut, which mimicked mildly alkaline and mildly acidic conditions, respectively. However, pH dependence was seen in the interaction propensity of H337-E349 and H337-D352. In the GB/0.1M/Mut simulation, in which H337 was protonated, short-range interactions of H337-E349 were present but less populated than R337-E349 in the corresponding GB/0.1M/Wt, due to histidine's shorter sidechain. On the other hand the H337–D352 interaction (the analog of the X-ray structures R337–D352 salt bridge) was retained in the mutant simulations with H337 protonated, independent of the solvent model or ionic strength. This interaction was almost non-existent in the GB/0.1M/Mut^{-} simulation, in which histidine was deprotonated. In the strong acid simulations, GB/0.1M/Wt+ and GB/0.1M/Mut+ all interactions weakened significantly in both wild-type and mutant simulations, although a small population of the R337–E349 interaction was observed. Similarly, in the case of explicit water simulations, the distributions of the R333–E349 and R333–D352 interactions were unaffected by mutation at 337. However, mutation mostly eliminated the H337–E349 interaction and re-established H337–D352 interaction that seemed to have been superseded by the three other ionic interactions in the wild-type simulations. This substantial loss of salt bridging in the strong-acid simulations probably contributed to the general deviation from the crystal structure.

Overall, both explicit and GB solvent models showed similar responses to mutation at R337 and to ionization-state changes corresponding to a passage from alkaline, to mildly acidic, to strongly acidic solution conditions. Moreover, the responses observed in the simulation correspond well to experimental observations, in which strong acid conditions destabilize the wild-type, while alkaline conditions destabilize R337H[22,38]. This serves to validate the use of GB to model the behavior of ionic interactions in this and similar systems.

Ionic interaction at dimer-dimer interface

It has been accepted from structural studies that the association of the two dimers into a tetramer is mostly stabilized by hydrophobic interactions. However the simulation results show that ionic interactions also occur across the dimer–dimer interface. In the wild-type GB simulations, R337 of monomer A on one dimer was found to interact with E343 of monomer C on the other dimer (see supplemental figures). This interaction is not seen in the starting crystal structure.

When the R337–E343 occurred, the R337–E349 interaction between monomers A and B disappeared but a partial interaction of R337-D352 remained. Four possible interactions of this kind (R337-E343) exist at interaction sites AC, CA, BD and DB; and interactions occurred at two of them, sites AC and DB. Surprisingly, interaction existed even in the acidic simulation where the sidechains of acidic residues were neutral. Visual inspection showed that the interaction was maintained through the sidechain carbonyl oxygen of the protonated E343. However no such interaction was observed in GB/0.0M/Wt, which again may suggest an ionic-strength or solvent-model dependence.

In addition to E343 on monomer C, R337 on monomer A made an ionic interaction with K351 on monomer B, an interaction that was also seen by NMR but not in the crystal structure[8,9]. Thus, E343 can interact with either R337 or K351. It can also interact with both at the same time. Unlike the R337-E343 interaction, the K351-E343 interaction was not observed in acidic conditions. However this interaction was observed in all non-acidic GB simulations for both the wild-type and the R337H mutant. In the case of explicit solvents however, only the wild-type had this interaction. Further details are shown in the supplemental figures.

The crystalline interface

Visual inspection of the trajectories showed that although the sidechain of R333 sometimes extended into solution in the simulations, it was much more often turned inwards. This raises the question of why an extended conformation is seen in the crystal structure. Inspection of the Jeffrey et al. crystal structure[9] shows that the extended R333 makes a salt bridge with E346 of another tetramer across the crystalline interface (Figure 6a and b). The R333-$N_{\eta 1}$ to E346-$O_{\varepsilon 1}$ distance in this interaction is only 2.62 Å. This crystal contact also exists in the crystal structure by Mittl and co-workers[11]. Also shown in figure 6A and B is Y327, which has an inter-monomer hydrogen bond with R333 as reported from crystallography[9]. As to whether this was maintained in the alternate “bent” form for the sidechain of R333, the distribution of the distance between the O_{η} atom of Y327 and the C_{ζ} atom of R333 during the simulations is shown in Figure 6C. All simulations had substantial populations in which this interaction was broken (distance > 5 Å) while the simulations that showed significant peaks near 4 Å are the same ones in which R333 was sometimes in extended conformations. Visual inspection of simulations shows that the R333–Y327 interaction occurs preferentially for extended conformers of R333. Finally, in the simulations, E346, lacking the crystal contact with R333, made the intra-monomer interaction with R342 which is involved in stabilizing the helix as mentioned previously.

We propose that the extended conformation of R333, somewhat stabilized by an interaction with Y327, is a minority population in solution, but that crystallization traps this conformation via the salt-bridging crystal contact with E346 of an adjacent tetramer.

Amide backbone hydrogen bonding

The fraction of time that each residue's backbone amide hydrogen atoms are involved in hydrogen bonds with backbone carbonyl groups is shown in Figure 7. The three distinct peaks (Phe328, Leu330 and Ile332) in the beta strand region arise from the hydrogen bonding between anti-parallel beta strands in a dimer. This finding is consistent with HD exchange experiments from Neira et al. and Galea et al. who both find slow exchange (high protection) for the amide groups of these residues[24,39].

The peak at G334 is in the turn region and arises from an H-bond with the backbone CO group of E326 on the other monomer of the dimer. This is at variance with the results of Neira et al., who find that the exchange is too rapid to measure at pH 7., but is somewhat more consistent

with the results of Galea et al. who find a measurably reduced, but still fast exchange rate at pH 4.0.

Residues 338 to 356 showed significant backbone H-bonding which arises from the helix within each monomer, with the degree of H-bonding tending to fall off at the C-terminal end. Although the H-bond frequency appears to be periodic, this periodicity has no apparent relation to whether the residues are exposed to the solvent or projecting towards the hydrophobic core. Rather, the peaks appear to arise from helix-stabilizing sidechain interactions noted above. The peaks at 339, 342 and 346 correspond to the ionic interactions of the R342 sidechain with E339 and E346. The sidechain of N345, where another peak occurred, is deeply buried in the dimer–dimer interface. The sidechains of E349 and D352, for which enhanced backbone amide H-bonding was also observed, are part of the aforementioned fluid salt-bridging network with R333 and R337. The weaker amide H-bonding observed for M340, L344 and L350 may be due to slight movements of hydrophobic core at the dimer–dimer interface, leading to straining of their corresponding backbone hydrogen bonds. The low point at E343 within the helix was caused by the E343 sidechain reaching across the dimer–dimer interface to either R337 or K351 leading to strain of the backbone H-bond. The gross features of H-bonding observed in the helical region in the simulation is in agreement with The H/D exchange results of both Neira et al. and Galea et al., which show enhanced protection of amide H-bonds in the helical region with protection decreasing towards the C-terminal end. However, the fine structure of somewhat more or less frequent H-bonding does not correspond with the more coarse-grained H/D exchange measurements.

The most notable difference in H-bonding in different simulations is between the explicit water simulations and the GB simulations with backbone H-bonding being significantly stronger in the latter. This may reflect a tendency for GB to overestimate protein–protein H-bonds due to lack of competition from explicit H-bonds to water. Otherwise, mutation and solution conditions did not strongly affect the frequency of backbone H-bonds.

MM/PBSA analysis

A relatively rapid computational alanine scanning approach introduced by Massova and Kollman[36] has been used to estimate the contribution of different sidechains to the stability of the tetramer. The method is based on the molecular-mechanics Poisson–Boltzmann surface-area method (MM/PBSA) in which snapshots are taken from a molecular dynamics simulation, and their energies are estimated using the molecular-mechanics force field for the vacuum contribution, Poisson–Boltzmann theory for the electrostatic component of solvation, and a surface-area based method for the non-polar component of solvation[40]. This method has been applied to the energetics of turn formation in peptides[41,42], interconversion of A- and B-form DNA, protein–drug binding[43-45] and protein–protein interaction[46]. Protein conformational entropy is typically estimated by normal-mode analysis.

In the Massova and Kollman method of applying MM/PBSA to the influence of mutations to alanine on protein–protein interaction free energy, snapshots are taken from a simulation of the wild-type complex, and each snapshot is subjected to the following procedure: MM/PBSA energies are calculated for the complex and for the isolated monomers making up the complex; each mutation site is in turn converted to alanine by truncation (without altering atom positions of any other residues in the snapshot), and MM/PBSA calculations are repeated for the “mutant” so constructed. Differences of differences of the complex and monomer energies with and without each of the mutations are then the predicted changes in the free-energy of association due to those mutations. Changes in protein conformational entropy are not included since they are likely to be small compared to other energy terms. An alternative procedure also explored by Massova and Kollman uses separate simulations of the complex and the monomers. Although more rigorous in principle than the single-simulation protocol, since it would allow

for some conformational changes upon dissociation, the multiple-simulations protocol does not result in cancellation of the fluctuations of energy terms internal to the monomers resulting in much larger RMS deviations of the calculated energy differences. Therefore, the single-simulation protocol (which is used here) is often preferred[36].

Because the tet-domain is a homotetramer, we have developed a variant of the method in which, for a particular site in the sequence, that site in all four monomers is truncated to alanine. This has been done, in turn, for all residues in the tet-domain except Gly, Pro and Ala residues. The results are presented in Table 2. The "all interface" character of the tet-domain is manifested in the fact that there are very few residues whose mutation has a negligible effect either in the calculations or experimentally. Only 7 of 26 mutations are calculated to have $|\Delta\Delta G_{fold}| < 2.0$ kcal/mol, and only 6 of 24 have experimental values this small.

The overall correlation of calculation to experiment is not particularly strong (Pearson correlation coefficient 0.50), however, if the polar and charged residues (Glu, Gln, Asp, Asn, Arg Lys) are treated in a separate class, a much stronger correlation is seen (correlation coefficient 0.72, Figure 8). The linear fit shows that the magnitude of the folding free energy change is overestimated by a factor of approximately 2.8. The tendency of computational alanine scanning by this or similar methods to over-estimate the effects of altering charged or polar residues has been noted by other workers, and the use of an interior dielectric constant in the range 2 to 4 (instead of 1, as in the present case) has been proposed[47,48]. Three of the four residues participating in the observed fluid salt-bridging system, Arg333, Arg337 and Glu349 are significant outliers. Most mutations to alanine are destabilizing both experimentally and according to computations. The most stabilizing mutation Glu326Ala, is correctly predicted to be stabilizing, but the other stabilizing mutation, Lys351Ala, is predicted to be destabilizing. For the five non-polar residues for which there is a measured $\Delta\Delta G_u$, the correlation between calculations and experiment is much weaker (0.48, scatter plot not shown). The computed folding free energy changes for these residues range from −7.2 to −1.7 kcal/mol, which is quite similar to the range of the experimental values (−7.3 to −2.1). For the five sites where mutation to alanine is found to result in an unfolded protein, the calculated values range from −5.1 to −3.7 kcal/mol. Thus, while the calculations for non-polar residues get approximately the correct magnitude, they do not reliably distinguish mutations that prevent folding from those that only destabilize the tetramer.

The standard MM/PBSA method for computational alanine scanning from a single wild-type simulation has several well-known shortcomings. Because the mutant species are never simulated, conformational re-arrangements in response to mutation cannot be accounted for. This consideration is particularly noteworthy for the observed salt-bridging system whose fluid character in the simulations suggests the ability to re-optimize pairings in response to mutation. Another limitation is that no simulation of the dis-associated state is performed. While this leads to a cancellation of fluctuations that improves precision, the neglect of the effects of conformational change upon dissociation, or more specifically, the effects of the mutation upon the effects of that conformational change, may be significant. Conceptually, the unfolding of the tet-domain can be divided into two thermodynamic steps: the dissociation of the tetramer into four monomers which retain a native-like, strand-turn-helix conformation, and the unfolding of these monomers. The use of a single simulation amounts to an approximation that the main effects of mutation will occur in the first step, while the effect of mutation will be smaller in the second step. The strong correlation for polar and charged residues is likely related to the fact, observable in the simulations, that the major polar and charged sidechain–sidechain interactions occur between monomers, not within them. Conversely, the non-polar sidechains may be making significant contributions to monomer secondary-structure stability as well as to tetramerization. These considerations are similar to those in the original introduction of the

technique by Massova and Kollman, as they studied the binding to MDM2 of a helical fragment of p53 that is likely to be significantly disordered in solution[36].

Recently, Chong et al.[32] performed a novel and very different kind of computational alanine scanning on the dimer form of the tet domain. For each considered alanine mutant, large numbers of high-temperature unfolding simulations were conducted using a grid computing system, and it was hypothesized that shorter average unfolding times (reduced *kinetic* stability) would be correlated with reduced thermodynamic stability. Many of the same charged and polar residues that are identified here by MM/PBSA as important for stability were also identified by their method, and they also had difficulty identifying the most destabilizing hydrophobic mutations.

Concluding remarks

The crystal structure of the tet domain of p53, together with the known sensitivity of the protein to mutations at position 337, implies a conventional picture of stabilization by a strong salt bridge between R337 and D352 at four equivalent sites. Here however, molecular dynamics simulation and close analysis of ionic interactions reveals four quartets of charged residues including these two and also R333 and E349, in four fluid salt-bridging systems in which partners are dynamically exchanged. This Swapping of the interactions can be seen to occur on the 1 to 10 ns timescale in Figure 4A(ii), but in some of the other interaction sites, some distance fluctuations were much more rapid (Figure 4A(iii)), while other distances remained short within a given interaction site throughout the 15 ns production runs. No pair remained at short distance throughout the entire simulation at all four interaction sites — all were subject to some degree of exchange. The slow rate of interaction-swapping relative to simulation time can be expected to make quantitative calculations of interaction energies problematic. The flexible nature of this system implies an ability to adapt to mutational losses by re-arranging salt bridges. Thus the effect of multiple mutations would be expected to be more complex than one- or two-body additivity.

The effect of the R337H mutation under mildly acidic conditions (His protonated) is to retain the 337–D352 interaction seen in the crystal structure, but to lose much of the interaction with E349 seen in the wild-type simulations. When His becomes deprotonated at higher pH, the interactions with 337 are also lost. This corresponds to the experimental finding that the mutant at pH 7 is slightly destabilized but still folded and functional, but much more strongly destabilized as the introduced His sidechain deprotonates at higher pH[22,26].

Similar patterns of exchangeable salt-bridging were seen in both explicit-water and implicit-solvent (GB) simulations. This supplies some validation for the use of GB to extend calculations to other conditions of pH and ionic strength as was done here, and also for future simulations in which GB models might be used to study the relative strengths of salt bridges. The closely-related MM/PBSA method appears to give a good correlation to experiment for the effects of ionic interactions, but tends to over-estimate the effects. Zoete et al.[49] have also found that implicit solvent models can givewell-behaved simulations but result in over-estimates of salt-bridge effects. The explanation may be that in response to mutation or unfolding, charged groups find other interactions not sampled in simulations of these kinds.

In simulations representing low-pH conditions (all acids protonated) we observe the beginnings of acid-induced unfolding without resorting to unphysical conditions, such as very high temperature or forcing along an “unfolding coordinate.” We have had a similar experiences with acid-unfolding simulations of myoglobin50. In the present case, the low-pH simulations take on many of the characteristics of the transition-state ensemble seen in previous studies[29,31], but does not unfold. This is to be expected in a simulation at 300 K since the experimental melting temperature at pH 3 is lowered only to 307 K[38]. Some of the most

dramatic effects of protonating the acidic sidechains are distortions in the largely hydrophobic dimerdimer interface, which suggests that the salt bridges observed in this interface involving E343, R337 and K351, may be important for proper orientation of the hydrophobic dimer surfaces and their partitioning away from water.

Methods

Except where otherwise noted, molecular modeling, dynamics simulations, and analysis were carried out using the Amber 8 suite of programs[51], and its force field, *ff99*[52] with the *mod_phipsi.1* correction to backbone torsional parameters[53]. In dynamics runs, the SHAKE algorithm was used to fix all bond lengths involving hydrogen, enabling the use of a 2 fs time step. Starting coordinates of the p53 tetramerization domain are taken from the X-ray structure of Jeffrey et al.[9] (pdb code 1C26; residues 325 to 356), which gives monomer coordinates and the transformation matrices necessary to generate the biologically relevant tetramer. The monomer was first capped with neutralizing end groups – ACE (Acetyl) and NME (N-Methyl), and then tetramerized using the provided transformations. Hydrogen atoms were added using the LEaP module of Amber. In order to obtain the mutant R337H, the monomeric crystal structure was mutated at R337 *in silico* to histidine using the side chain conformation prediction program, SCWRL3[54]. The mutant monomer was then capped and tetramerized as described above for the wild type. All calculations were done on the Hartwell Centers IBM/Linux Blade cluster.

Explicit water simulations

The net charge of the tetramer was neutralized by adding sodium ions to the simulation cell. Crystallographic waters were retained and additional TIP3P[55] water molecules were added to fill a truncated octahedral box, resulting in a total of 4051 waters. Particle mesh Ewald (PME) with periodic boundary condition was used to calculate the long range interactions, setting the real space cut off to 10.0 Å. The temperature was regulated by Langevin dynamics with collision frequency of 1.0 ps^{-1}. Minimization was performed in two stages. First the solvent and ions were minimized for 5000 steps, holding the protein fixed with a high harmonic constant such as 500 kcal mol^{-1} $Å^{-2}$. Then the whole system was minimized for 10000 steps. Both stages of minimization started with 1000 steepest descent steps while the remaining steps were conjugate gradient. The system was then heated at constant volume to 300K over 60 ps, keeping the tetramer fixed with a weak restraint of 10 kcal mol^{-1} $Å^{-2}$. Equilibration was also performed in two stages to eliminate the unfavorable cavities in the bulk water. First water molecules were equilibrated under constant NPT conditions for 60 ps with 2 fs time step. The tetramer was kept restrained at this stage. Then the whole system was equilibrated for 100 ps under constant NPT condition again. After equilibration, a solvent density of 1.04 g/cc was achieved and the resulting box size was fixed for the subsequent constant-NVT equilibration and production simulation. The equilibration and production dynamics simulations were performed using the PMEMD module[56] in Amber8.

Generalized Born simulations

Solvent effects were modelled implicitly with the generalized Born model-II of Onufriev et al.[35], which is implemented in Amber 8. The dielectric constants of 1 and 78.5 were used for the protein interior and solvent regions, respectively. The non-polar solvation free energy was calculated using the solvent accessible surface area model[57] with a surface tension of 0.005 kcal mol^{-1} $Å^{-2}$. The tetramer was first minimized under this energy function with 10,000 steps of conjugate gradient minimization. It was then heated to 300 Kelvin using 1.0 fs time step for 30 ps. All protein residues were restrained using a 1 kcal mol^{-1} $Å^{-2}$ harmonic restraint during the heating process. Then the whole system was equilibrated for 1 ns without restraints, followed by the production runs. Salt effects were included using an extension of the GB model

to include Debye-Hückel theory[37]. Temperature was regulated through use of Langevin dynamics with a collision frequency of 0.5 ps^{-1} [58,59]. The cut-off distances for both non-bonded interaction and Born-radius calculation were set at 16 Å.

Computational alanine scanning

An MM/PBSA procedure based on that of Massova and Kollman[36] has been used to estimate the effect on tetramer stability of mutating individual sidechains to alanine. Here a variant of the procedure suited to a homotetramer is used in which, for a given sequence position, the mutation to alanine is done on all four monomers simultaneously. This procedure has been implemented locally as a Python program. The program implements the Amber vacuum energy function as encoded in the "parmtop" files generated by the LEaP module of Amber, uses DelPhi[60,61] for the Poisson–Boltzmann calculations and an adaptation of the Amber molsurf program for surface areas.

As in the the original method, protein conformational entropy is omitted, while solvent entropy is included implicitly in the solvation model. Thus, the change in folding free energy due to an alanine mutation is

$$\Delta\Delta G_{\mathrm{fold}} = \left\langle W(\mathrm{mut,\ tet}) - W(\mathrm{wild,\ tet}) - \sum_{i=1}^{4} [W(\mathrm{mut,\ mono}\ i) - W(\mathrm{wild,\ mono}\ i)] \right\rangle,$$

where the averaging is done over coordinate snapshots and W is the potential of mean force that is estimated for a particular value of the solute coordinates, q,

$$W(q) = E_{\mathrm{MM}}(q) + \Delta G_{\mathrm{sol,elec}}(q) + \Delta G_{\mathrm{sol,np}}(q).$$

where $E_{\mathrm{MM}}(q)$ is the instantaneous vacuum energy of solute in conformation q, and is given by the molecular-mechanics potential energy function; $\Delta G_{\mathrm{sol,elec}}(q)$ is the electrostatic component of the free energy of solvation of the solute in conformer q; and $\Delta G_{\mathrm{sol,np}}(q)$ is the non-polar component. The coordinates for both tetramer and monomer are taken from the tetramer simulation after stripping solvent molecules, and mutant coordinates are generated by truncating the considered sidechain to alanine, adding the appropriate hydrogen atoms, and setting atomic partial charges to those of alanine. $\Delta G_{\mathrm{sol,elec}}(q)$ is calculated by the finite-difference Poisson–Boltzmann method using DelPhi with a 0.5 Å grid spacing and the induced surface charges method of calculating the reaction field[61]. $\Delta G_{\mathrm{sol,np}}(q)$ is estimated as a linear function of the solvent-accessible surface area (SASA)[57], $\Delta G_{\mathrm{sol,np}}(q) = \gamma\mathrm{SASA} + \sigma$ with γ = 0.00542 kcal mol^{-1} $Å^{-2}$, σ = 0.92 kcal/mol. The simulation used for input was Explicit/Wt. The vacuum potential was that used in the simulation but with no periodic boundary conditions or cutoffs.

Supplementary Material

Refer to Web version on PubMed Central for supplementary material.

References

1. Bullock AN, Fersht AR. Rescuing the function of mutant p53. Nat. Rev. Cancer 2001;1:68–76. [PubMed: 11900253]
2. Hainaut P, Hollstein M. p53 and human cancer: the first ten thousand mutations. Adv Cancer Res 2000;77:81–137. [PubMed: 10549356]
3. Kastan MB, Onyekwere O, Sidransky D, Vogelstein B, Craig RW. Participation of p53 protein in the cellular response to DNA damage. Cancer Res 1991;51:6304–6311. [PubMed: 1933891]
4. Lane DP. p53, guardian of the genome. Nature 1992;358:15–16. [PubMed: 1614522]

5. Graeber TG, Osmanian C, Jacks T, Housman DE, Koch CJ, Lowe SW, Giaccia AJ. Hypoxia-mediated selection of cells with diminished apoptotic potential in solid tumours. Nature 1996;379:88–91. [PubMed: 8538748]
6. Lee WT, Harvey TS, Yin Y, Yau P, Litchfield D, Arrowsmith CH. Solution structure of the tetrameric minimum transforming domain of p53. Nat. Struct. Biol 1994;1:877–890. [PubMed: 7773777]
7. Clore GM, Omichinski JG, Sakaguchi K, Zambrano N, Sakamoto H, Appella E, Gronenborn AH. High-resolution structure of the oligomerization domain of p53 by multidimensional NMR. Science 1994;265:386–391. [PubMed: 8023159]
8. Clore GM, Ernst J, Clubb R, Omichinski JG, Kennedy WM, Sakaguchi K, Appella E, Gronenborn AM. Refined solution structure of the oligomerization domain of the tumour suppressor p53. Nat Struct Biol 1995;2:253–254. [PubMed: 7796256]
9. Jeffrey PD, Gorina S, Pavletich NP. Crystal structure of the tetramerication domain of the p53 tumor suppressor at 1.7 Ångstroms. Science 1995;267:1498–1502. [PubMed: 7878469]
10. Miller M, Lubkowski J, Rao JK, Danishefsky AT, Omichinski JG, Sakaguchi K, Sakamoto H, Appella E, M GA, Clore GM. The oligomerization domain of p53: crystal structure of the trigonal form. FEBS Lett 1996;399:166–170. [PubMed: 8980144]
11. Mittl PR, Chene P, Grutter MG. Crystallization and structure solution of p53 (residues 326-356) by molecular replacement using an NMR model as template. Acta Crystallogr D Biol Crystallogr 1998;54:86–89. [PubMed: 9761820]
12. Chène P. The role of tetramerization in p53 function. Oncogene 2001;20:2611–2617. [PubMed: 11420672]
13. Balagurumoorthy P, Sakamoto H, Lewis MS, Zambrano N, Clore GM, Gronenborn AM, Appella E, Harrington RE. Four p53 DNA-binding domain peptides bind natural p53-response elements and bend the DNA. Proc Natl Acad Sci U S A 1995;92:8591–8495. [PubMed: 7567980]
14. Nagaich AK, Zhurkin VB, Durell SR, Jernigan RL, Appella E, Harrington RE. p53-induced DNA bending and twisting: p53 tetramer binds on the outer side of a DNA loop and increases DNA twisting. Proc Natl Acad Sci U S A 1999;96:1875–1880. [PubMed: 10051562]
15. Kawaguchi T, Kato S, Otsuka K, Watanabe G, Kumabe T, Tominaga T, Yoshimoto T, Ishioka C. The relationship among p53 oligomer formation, structure and transcriptional activity using a comprehensive mis-sense mutation library. Oncogene 2005;24:6976–6981. [PubMed: 16007150]
16. Shieh SY, Ahn J, Tamai K, Taya Y, Prives C. The human homologs of checkpoint kinases Chk1 and Cds1 (Chk2) phosphorylate p53 at multiple DNA damage-inducible sites. Genes Dev 2000;14:289–300. [PubMed: 10673501]Erratum in: Genes Dev 2000 Mar 15;14(6):750
17. Kubbutat MH, Ludwig RL, Ashcroft M, Vousden KH. Regulation of Mdm2-directed degradation by the C terminus of p53. Mol. Cell. Biol 1998;18:5690–5698. [PubMed: 9742086]
18. Maki CG. Oligomerization is required for p53 to be efficiently ubiquitinated by MDM2. J. Biol. Chem 1999;274:16531–16535. [PubMed: 10347217]
19. Delphin C, Huang KP, Scotto C, Chapel A, Vincon M, Chambaz E, Garin J, Baudier J. The in vitro phosphorylation of p53 by calcium-dependent protein kinase C. characterization of a protein-kinase-C-binding site on p53. Eur. J. Biochem 1997;245:684–692. [PubMed: 9183006]
20. Dobner T, Horikoshi N, Rubenwolf S, Shenk T. Blockage by adenovirus E4orf6 of transcriptional activation by the p53 tumor suppressor. Science 1996;272:1470–1473. [PubMed: 8633237]
21. Stommel JM, Marchenko ND, Jimenez GS, Moll UM, Hope TJ, Wahl GM. A leucine-rich nuclear export signal in the p53 tetramerization domain: regulation of subcellular localization and p53 activity by NES masking. EMBO J 1999;18:1660–1672. [PubMed: 10075936]
22. DiGiammarino EL, Lee AS, Cadwell C, Zhang WX, Bothner B, Ribeiro RC, Zambetti G, Kriwacki RW. A novel mechanism of tumorigenesis involving pH-dependent destabilization of a mutant p53 tetramer. Nat. Struct. Biol 2002;9:12–16. [PubMed: 11753428]
23. Lee A, Galea C, DiGiammarino E, Jun B, Murti G, Ribeiro R, Zambetti G, Schultz C, Kriwacki R. Reversible amyloid formation by the p53 tetramerization domain and a cancer-associated mutant. J. Mol. Biol 2003;327:699–709. [PubMed: 12634062]
24. Galea C, Bowman P, Kriwacki R. Disruption of an inter-monomer salt bridge in the p53 tetramerization domain results in an increased propensity to form amyloid fibrils. Protein Science 2005;14:2993–3003. [PubMed: 16260757]

25. Mateu MG, Fersht AR. Nine hydrophobic side chains are key determinants of the thermodynamic stability and oligomerization status of tumour suppressor p53 tetramerization domain. EMBO J 1998;15:2748–2758. [PubMed: 9582268]
26. Ribeiro R. An inherited p53 mutation that contributes in a tissue-specific manner to pediatric adrenal cortical carcinoma. PNAS 2001;98:9330–9335. [PubMed: 11481490]
27. Higashimoto Y, Asanomi Y, Takakusagi S, Lewis MS, Uosaki K, Durell SR, Anderson CW, Appella E, K. S. Unfolding, aggregation, and amyloid formation by the tetramerization domain from mutant p53 associated with lung cancer. Biochemistry 2006;45:1608–1619. [PubMed: 16460008]
28. Nicholls CD, McLure KG, Shields MA, Lee PW. Biogenesis of p53 involves cotranslational dimerization of monomers and posttranslational dimerization of dimers. implications on the dominant negative effect. J Biol Chem 2002;277:12937–12945. [PubMed: 11805092]
29. Mateu MG, Sanchez Del Pino MM, Fersht AR. Mechanism of folding and assembly of a small tetrameric protein domain from tumor suppressor p53. Nat Struct Biol 1999;6:191–198. [PubMed: 10048932]
30. Chong LT, Snow CD, Rhee YM, Pande VS. Dimerization of the p53 oligomerization domain: identification of a folding nucleus by molecular dynamics simulations. J Mol Biol 2005;345:869–878. [PubMed: 15588832]
31. Duan J, Nilsson L. Thermal unfolding simulations of a multimeric protein–transition state and unfolding pathways. Proteins 2005;59:170–182. [PubMed: 15723359]
32. Chong LT, Swope WC, Pitera JW, Pande VS. Kinetic computational alanine scanning: application to p53 oligomerization. J Mol Biol 2006;357:1039–1049. [PubMed: 16457841]
33. Tompa P. Intrinsically unstructured proteins. Trends Biochem Sci 2002;27:527–533. [PubMed: 12368089]
34. Dyson HJ, Wright PE. Coupling of folding and binding for unstructured proteins. Curr. Opin. Struct. Biol 2002;12:54–60. [PubMed: 11839490]
35. Onufriev A, Bashford D, Case DA. Exploring protein native states and large-scale conformational changes with a modified generalized born model. Proteins 2004;55:383–394. [PubMed: 15048829]
36. Massova I, Kollman PA. Computational alanine scanning to probe protein–protein interactions: A novel approach to evaluate binding free energies. J. Am. Chem. Soc 1999;121:8133–8143.
37. Srinivasan J, Trevathan MW, Beroza P, Case DA. Application of a pairwise generalized Born model to proteins and nucleic acids: inclusion of salt effects. Theor. Chem. Acc 1999;101:426–434.
38. Johnson CR, Morin PE, Arrowsmith CH, Freire E. Thermodynamic analysis of the structural stability of the tetrameric oligomerization domain of p53 tumor suppressor. Biochemistry 1995;34:5309–5316. [PubMed: 7727392]
39. Neira JL, Mateu MG. Hydrogen exchange of the tetramerization domain of the human tumour suppressor p53 probed by denaturants and temperature. Eur. J. Biochem 2001;268:4868–4877. [PubMed: 11559355]
40. Kollman PA, Massova I, Reyes C, Kuhn B, Huo S, Chong L, Lee M, Lee T, Duan Y, Wang W, Donini O, Cieplak P, Srinivasan J, Case DA, Cheatham TE III. Calculating structures and free energies of complex molecules: Combining molecular mechanics and continuum models. Acc. Chem. Res 2000;33:889–897. [PubMed: 11123888]
41. Bashford D, Case DA, Choi C, Gippert GP. A computational study of the role of solvation effects in reverse turn formation in the tetrapeptides APGD and APGN. J. Am. Chem. Soc 1997;119:4964–4971.
42. Demchuk E, Bashford D, Gippert GP, Case DA. Thermodynamics of a reverse turn motif. solvent effects and side-chain packing. J. Mol. Biol 1997;270:305–317. [PubMed: 9236131]
43. Srinivasan J, Cheatham TE, Kollman PA, Case DA. Continuum solvent studies of the stability of DNA, RNA, and phosphoramidate–DNA helices. J. Am. Chem. Soc 1998;120:9401–9409.
44. Wang J, Morin P, Wang W, Kollman PA. Use of MM-PBSA in reproducing the binding free energies to HIV-1 RT of TIBO derivatives and predicting the binding mode to HIV-1 RT of of efavirenz by docking and MM-PBSA. J. Am. Chem. Soc 2001;123:5221–5230. [PubMed: 11457384]
45. Huo S, Wang J, Cieplak P, Kollman PA, Kuntz ID. Molecular and free energy analysis of cathepsin D–inhibitor interactions: Insight into structure-based ligand design. J. Med. Chem 2002;45:1412–1419. [PubMed: 11906282]

46. Gohlke H, Kiel C, Case DA. Insights into protein–protein binding by binding free energy calculation and free energy decomposition for the Ras–Raf and Ras–RalGDS complexes. J. Mol. Biol 2003;330:891–913. [PubMed: 12850155]
47. Archontis G, Simonson T, Karplus M. Binding free energies and free energy components from molecular dynamics and Poisson–Boltzmann calculations: application to amino acid recognition by aspartyl tRNA synthetase. J. Mol. Biol 2001;306:307–327. [PubMed: 11237602]
48. Moreira IS, Fernandes PA, Ramos MA. Computational alanine scanning mutagenesis–an improved methodological approach. J. Comput. Chem 2006;28:644–654. [PubMed: 17195156]
49. Zoete V, Meuwly M. Importance of individual side chains for the stability of a protein fold: Computational alanine scanning of the insulin monomer. J. Comput. Chem 2006;27:1843–1857. [PubMed: 16981237]
50. Onufriev A, Case DA, Bashford D. Structural details, pathways, and energetics of unfolding apomyoglobin. J. Mol. Biol 2003;325:555–567. [PubMed: 12498802]
51. Case, DA.; Darden, TA.; Cheatham, TE., III; Simmerling, CL.; Wang, J.; Merz, KM.; Duke, RE.; Pearlman, DA.; Caldwell, JW.; Ross, WS.; Stanton, RV.; Cheng, AL.; Vincent, JJ.; Crowley, M.; Tsui, V.; Gohlke, H.; Radmer, RJ.; Seibel, GL.; Singh, UC.; Weiner, PK.; Kollman, PA. AMBER 8. University of California; San Francisco: 2004.
52. Wang J, Cieplak P, Kollman PA. How well does a restrained electrostatic potential (RESP) model perform in calculating conformational energies of organic and biological molecules? J. Comput. Chem 2000;21:1049–1074.
53. Simmerling C, Strockbine B, Roitberg AE. All-atom structure prediction and folding simulations of a stable protein. J. Am. Chem. Soc 2002;124:11258–11259. [PubMed: 12236726]
54. Canutescu AA, Shelenkov AA, Dunbrack J. A graph theory algorithm for protein side-chain prediction. Protein Science 2003;12:2001–2014. [PubMed: 12930999]R. L.
55. Jorgensen WL, Chandrasekhar J, Madura J, Klein M. Comparison of simple potential functions for simulating liquid water. J. Chem. Phys 1983;79:926–935.
56. Duke, RE.; Pedersen, LG. PMEMD 3. University of North Carolina-chapel Hill; 2003. Technical report
57. Weiser J, Shenkin PS, Still WC. Approximate atomic surfaces from linear combinations of pairwise overlaps (LCPO). J. Comput. Chem 1999;20:217–230.
58. Pastor RW, Brooks BR, Szabo A. An analysis of the accuracy of Langevin and molecular-dynamics algorithms. Mol. Phys 1988;65:1409–1419.
59. Loncharich RJ, Brooks BR, Pastor RW. Langevin dynamics of peptides - the frictional dependence of isomerization rates of N-acetylalanyl-N'-methylamide. Biopolymers 1992;32:523–535. [PubMed: 1515543]
60. Rocchia W, Alexov E, Honig B. Extending the applicability of the nonlinear Poisson–Boltzmann equation: Multiple dielectric constants and multivalent ions. J. Phys. Chem. B 2001;105:6507–6514.
61. Rocchia W, Sridharan S, Nicholls A, Alexov E, Chiabrera A, Honig B. Rapid grid-based construction of the molecular surface and the use of induced surface charges to calculate reaction field energies: Application to the molecular systems and geometric objects. J. Comp. Chem 2002;23:128–137. [PubMed: 11913378]
62. Olivier M, Eeles R, Hollstein M, Khan M, Harris C, Hainaut P. The IARC TP53 database: new online mutation analysis and recommendations to users. Hum Mutat 2002;19:607–614. [PubMed: 12007217]

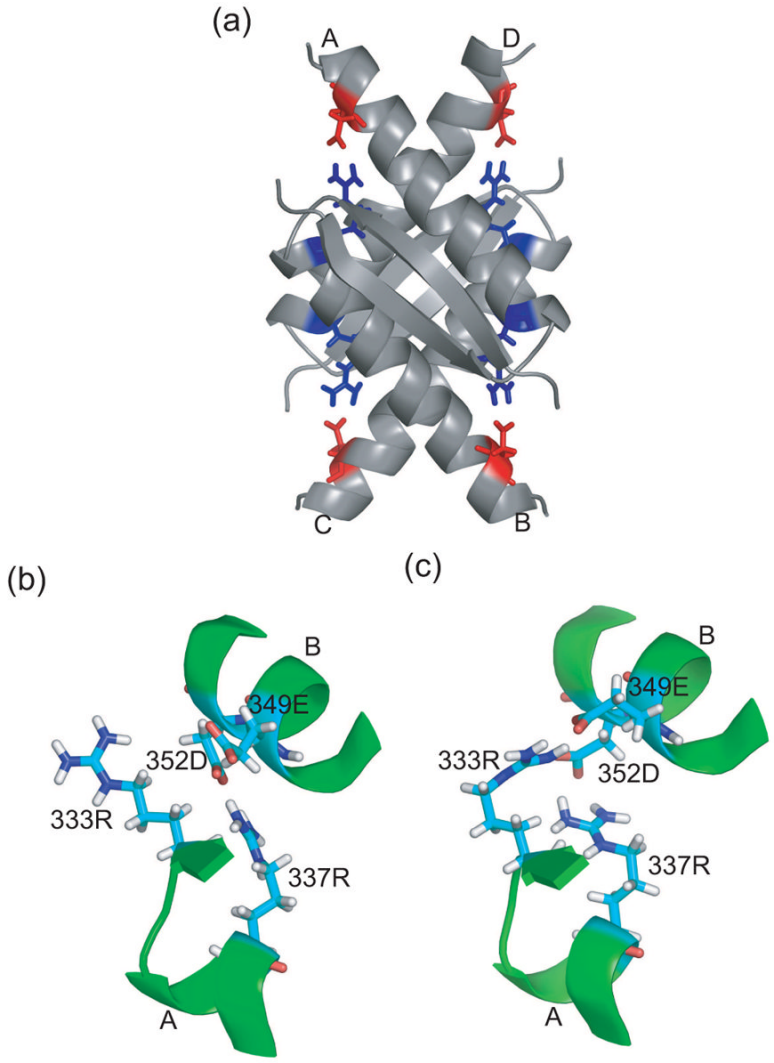

Fig. 1.

(a) The crystal structure of the p53 tet domain[9]. Locations of the salt bridge interactions between R337 (blue) and D352 (red) at the four interaction sites are shown. Since each monomer consists of the same residues, the monomer labels A, B, C and D are used to distinguish the residues when necessary. Nomenclature for interaction sites: the site where R337 on monomer A interacts with D352 on monomer B, is designated as site AB, while the the site where R337 on monomer B interacts with D352 on monomer A is designated BA. An analogous nomenclature is used for interaction sites CD and DC. (b) One of the interaction sites in the crystal structure, AB, along with relative orientations of R333 and E349. The side chain of R333 extends into the solution. (c) During the simulation, the guanidinium head of R333 turns in and interacts with E349 and D352.

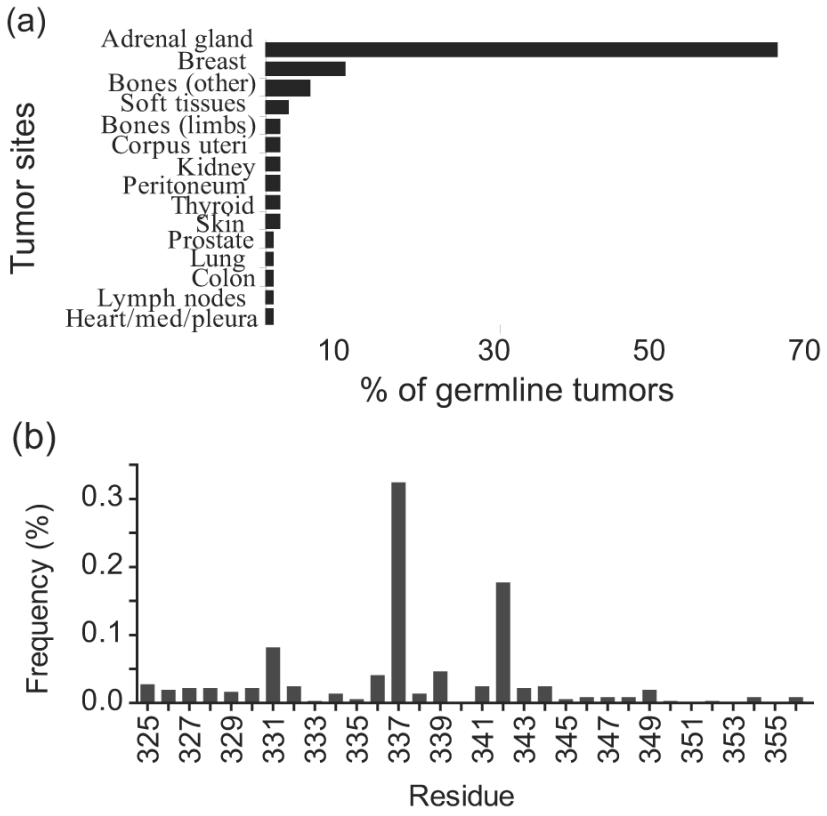

Fig. 2.

Tumors reported to be associated with mutations in the tet domain, based on analysis of data compiled in the IARC TP53 database as of August 2007 (http://www-p53.iarc.fr)[62]. (a) different locations of tumor occurrence versus percentage for germline mutation (108 cases); and (b) Frequency of mutation (both germline and somatic) in each residue (367 cases).

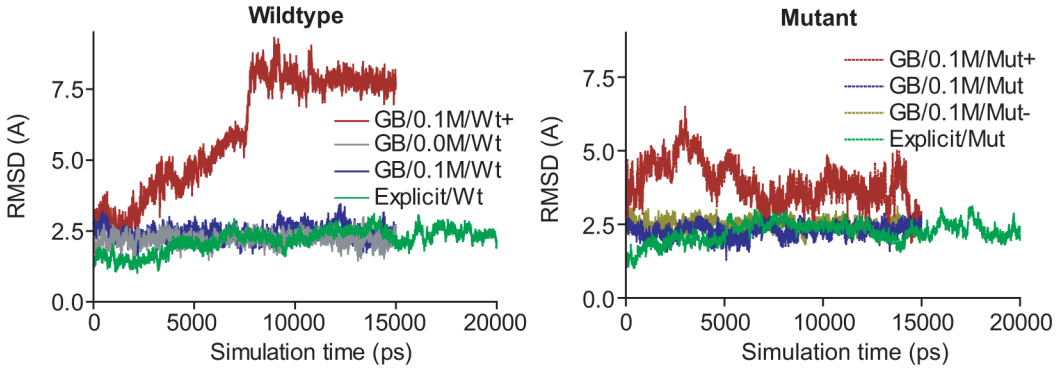

Fig. 3.

Backbone RMSD with respect to the crystal structure for all simulations. All heavy atoms (C, CA, N, O) in the backbone were considered.

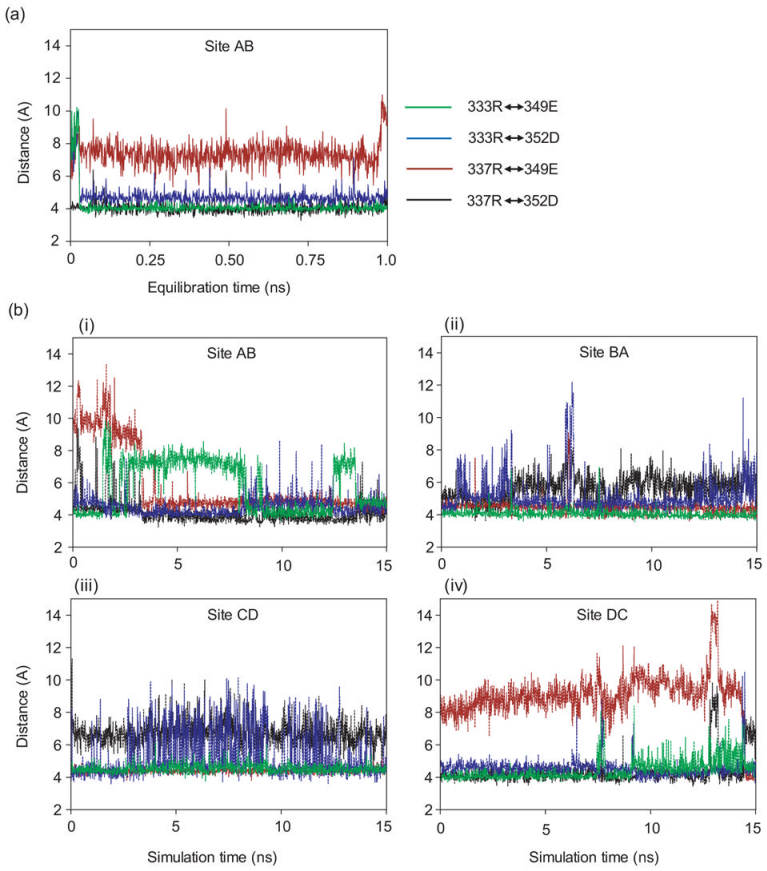

Fig. 4.

Instantaneous distances of the four salt-bridge interactions in the GB/0.1M/Wt simulation during: (a) equilibration at the site where R337 or R333 on monomer A interacts with acidic residues on monomer B; and (b) production run at all four different interaction sites. see Figure 1 for the interaction-site nomenclature.

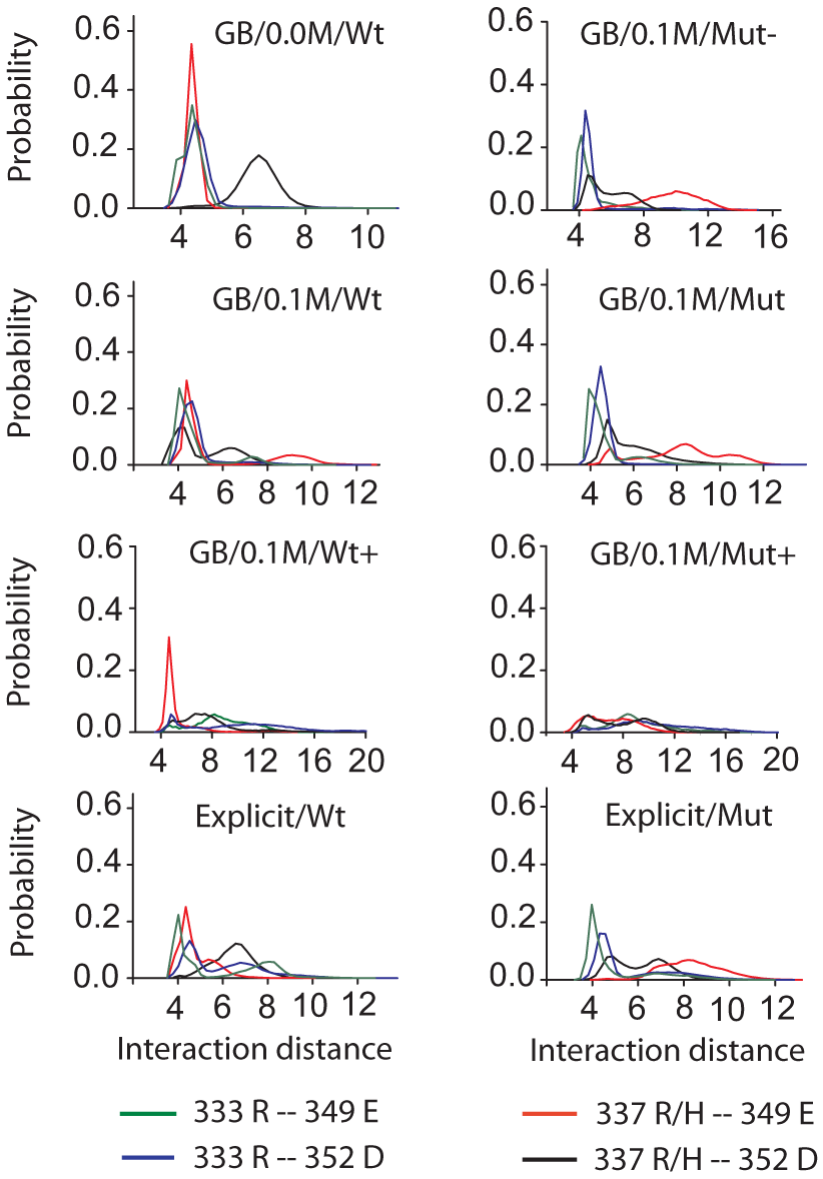

Fig. 5.

Distance distributions for specific salt bridges for all eight different simulation conditions. A bin size of 0.25 Å was used. Data was gathered from all four interaction sites.

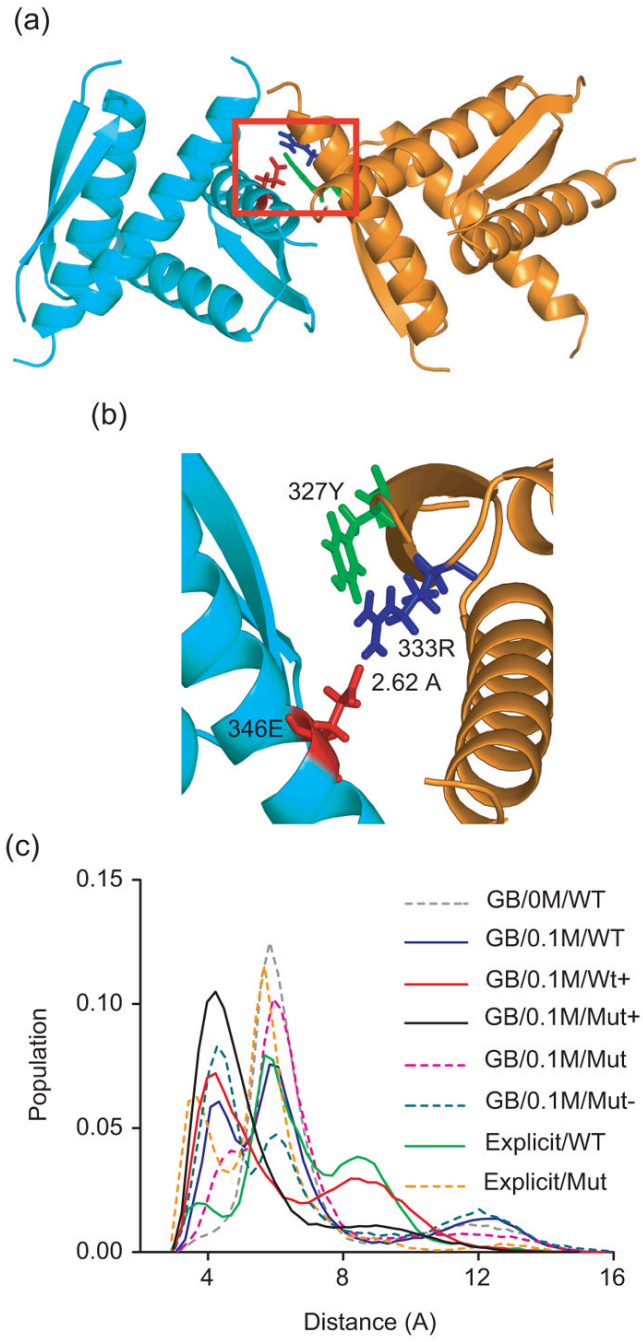

Fig. 6.

(a) Two tetramers are placed side by side, using the transformation matrix given in 1C26 pdb file, to illustrate the interaction at crystalline interface. (b) Looking down from the top of (a), interaction between E346 from one tetramer and R333 from another tetramer can been seen. (c) Distance distribution of the R333–Y327 inter-monomer interaction. The peak around 4 Å is the H-bonded population.

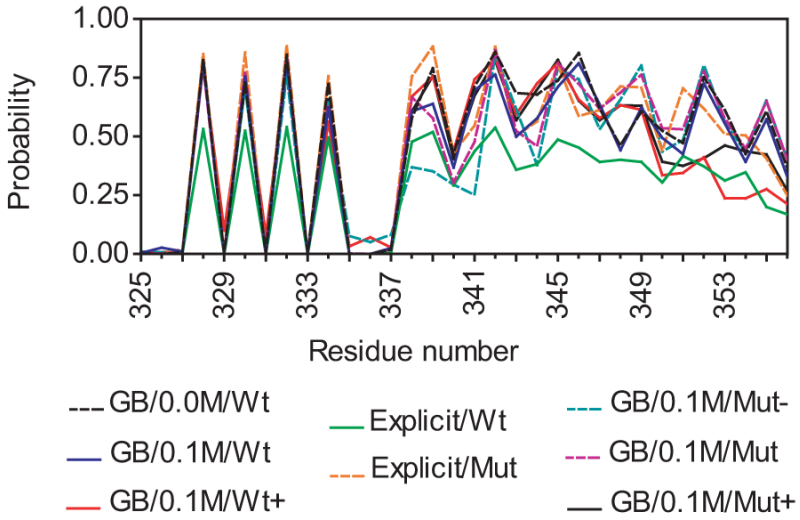

Fig. 7.

Backbone amide hydrogen bonding in the tetramer. Amide hydrogen bonding is defined as an N–O distance < 3.2 Å and an NHO angle ≥ 145°

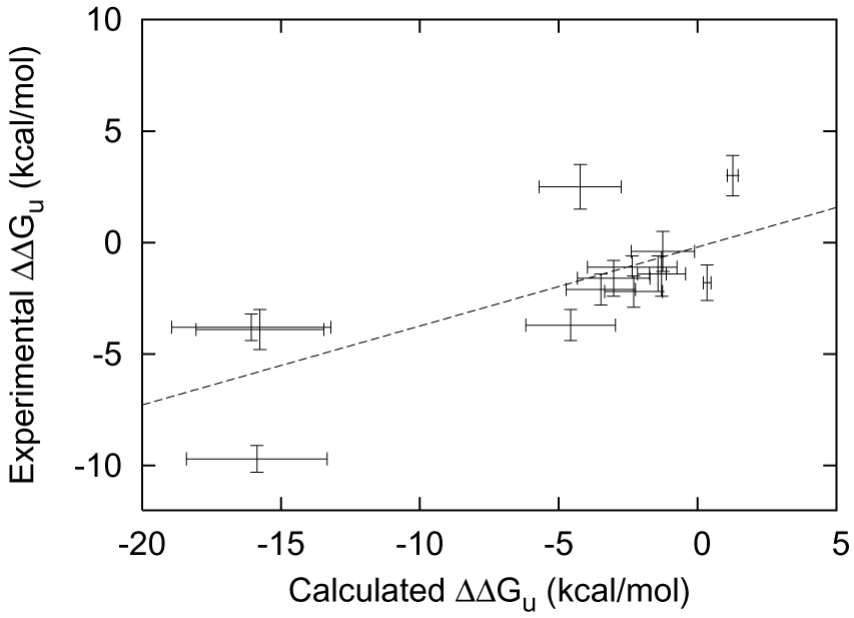

Fig. 8.

Scatter plot of calculated versus experimental changes in unfolding free energy upon mutation of polar or charged residues to Alanine. Data from Table 2. Best fit line: $y = x/2.82 - 0.20$. Correlation coefficient: 0.72.

Table 1

Simulation conditions and their abbreviations

Simulation conditions	Abbreviation	pH
GB, wildtype, 0.0 M	GB/0.0M/Wt	Neutral
GB, wildtype, 0.1 M	GB/0.1M/Wt	Neutral
GB, wildtype, 0.1 M, acidic residues protonated	GB/0.1M/Wt+	Acidic
GB, mutant, 0.1 M, H337 deprotonated	GB/0.1M/Mut−	Neutral
GB, mutant, 0.1 M, H337 protonated	GB/0.1M/Mut	Slight acidic
GB, mutant, 0.1 M, H337 & acidic residues protonated	GB/0.1M/Mut+	Acidic
Explicit water, wildtype	Explicit/Wt	Neutral
Explicit water, mutant, H337 protonated	Explicit/Mut	Slight acidic

Table 2

Computational Alanine Scanning by MM/PBSA

Mutated Site	Calculated[a]	Experimental[b]
Glu-326	−3.0(1.3)	−1.6(0.8)
Tyr-327	−3.3(0.6)	no data
Phe-328	−4.9(0.7)	−7.2(0.7)
Thr-329	−1.7(0.7)	−3.6(0.7)
Leu-330	−5.0(0.5)	unfolded
Gln-331	−1.3(0.9)	−1.4(1.0)
Ile-332	−3.7(0.5)	unfolded
Arg-333	−15.8(2.3)	−3.9(0.9)
Arg-335	−3.5(1.2)	−2.1(0.7)
Glu-336	1.3(0.2)	3.0(0.9)
Arg-337	−15.9(2.5)	−9.7(0.6)
Phe-338	−3.2(0.4)	−7.3(0.6)
Glu-339	0.3(0.1)	−1.8(0.8)
Met-340	−2.1(0.4)	−6.4(0.7)
Phe-341	−5.1(0.4)	unfolded
Arg-342	−1.4(0.3)	−1.4(0.8)
Glu-343	−2.4(1.6)	−1.1(0.5)
Leu-344	−3.7(0.4)	unfolded
Asn-345	−4.6(1.6)	−3.7(0.7)
Glu-346	−1.2(1.1)	−0.4(0.9)
Leu-348	−4.2(0.5)	unfolded
Glu-349	−16.1(2.9)	−3.8(0.6)
Leu-350	−2.9(0.6)	−2.1(0.7)
Lys-351	−4.2(1.5)	2.5(1.0)
Asp-352	−2.3(1.0)	−2.2(0.7)
Gln-354	−0.7(0.4)	no data

[a] The present calculations using MM/PBSA with RMSD in parenthesis. Each mutation to alanine was done on all four monomers at once and the calculated $\Delta\Delta G_u$ are divided by four to be on a per-monomer basis for comparison with experiment.

[b] The negatives of the $\Delta\Delta G_u$ extrapolated to zero denaturant concentration with error estimates in parenthesis as given in [b] of ref. [25]